OPTIMUM FUEL CONSUMPTION STRATEGY FOR SERIES-PARALLEL HYBRID ELECTRIC VEHICLES: MODELLING AND APPROACHES

Ivan Miguel Trindade[(a)], Agenor de Toledo Fleury[(b)]

[(a)] AVL Schrick GmbH, Germany
[(b)] Mechanical Engineering Department, Escola Politecnica, University of Sao Paulo, Brazil

[(a)]ivan.trindade@avl.com, [(b)] agenorfleury@usp.br

ABSTRACT

Hybrid Electric Vehicles (HEVs) present a wide range of powertrain configurations, degrees of hybridization and added costs when compared to conventional vehicles. From the point of view of control design, the major challenge is the reduction of fuel consumption and emissions. Methods for determining the energy management strategy that best suits this challenge relies on dynamic optimization techniques that find optimal values for the control variables depending on the system states and on the cost functions.

On the other hand, finding optimal control solutions is useless if the problem is not based on a reliable dynamic model of the system. This paper extends other works by the authors (Trindade, Fleury and Vogelaar, 2014; Trindade and Fleury, 2015) showing the steps for building a very detailed model of a Series-Parallel HEV in MATLAB™ and its identification using data available in the open literature. Afterwards, a Dynamic Programming technique is employed to explore optimal fuel consumption solutions to be compared to the 'non optimal one'. In the first approach, the optimal solution is obtained considering that the Internal Combustion Engine (ICE) follows its best fuel consumption curves and a considerable reduction against the 'non optimal' solution is achieved. Last but not least, in a second approach, the ICE is set not to follow a pre-optimized operating line and this leads to better results when compared to the first optimal approach.

Keywords: hybrid electric vehicle, dynamic programming, optimization

1. INTRODUCTION

While in the powertrain of a conventional vehicle all the driver power demand has to be fulfilled by the engine, in a hybrid vehicle an additional degree of freedom is introduced in the system by the addition of an electric motor. This extra degree of freedom is responsible for enabling hybrid functions, namely electric only propulsion, hybrid generation, hybrid boost and braking energy recuperation. Choosing the appropriate torque demand for electric motor and engine during the cycle is a task of the hybrid control strategy, which has to comply with the necessary performance, emission and fuel consumption requirements. This control strategy is referred in this paper as an Energy Management Strategy with the focus on fuel consumption reduction.

According to the literature, energy management strategies for hybrid powertrains are usually divided into two classes. Desai (2010), Salmasi (2007) and Zhu et al. (2004) classify control strategies into optimal control, which aims to minimizing the fuel consumption by choosing the appropriate control variables, and rule-based control, that controls the powertrain with the use of classic control rules not based on optimization methods. Several authors have shown the use of global optimal control theory applied to a hybrid powertrain, see Sundström (2009), Karbowski et al. (2009), Liu and Peng (2006) and Carignano, Nigro and Junco (2015). Global optimal control is implemented using previous knowledge of the driving route since the cost function aims to optimizing the fuel consumption consumed at the end of the cycle. Therefore, it is not a real-time implementable strategy, but provides the control variables that guarantee that the minimum fuel consumption is achieved.

Different drivetrain configurations for HEVs can accomplish the task of minimizing fuel consumption. The powertrain configuration of this study is a series-parallel electric hybrid which uses a planetary gear set to interconnect the ICE and two electric motors. This paper describes the development of two computational models of the hybrid powertrain: a highly detailed model using heuristic control (Trindade, 2016) and an optimal control model using Dynamic Programming (DP) routine in order to evaluate the full fuel consumption benefit of the system. Two cases of the DP model were simulated: one aiming to optimize only the split of power between battery and fuel; and another were the engine start event and the engine operating points were subject of optimization. The driving cycle FTP75 was used in the simulations since data for this route is available in the literature from dynamometer testing.

Preliminary results of this study (Trindade and Fleury, 2015) have pointed out for the importance of

having a small time step size in the dynamic programming routine in order to achieve results comparable to real-world systems. The improved results and the consequent findings will be presented in this paper.

2. DESCRIPTION OF THE POWERTRAIN SYSTEM

The configuration of the powertrain is shown in Figure 1, where a planetary gear set is a transmission component and is used to connect the following components: motor-generator 1 (MG1) to solar gear, ICE to carrier gear and motor-generator 2 (MG2) to ring gear. The ring gear is directly connected to the final gear and to the differential. The ratio of torque amplification from the ICE to the wheels is fixed by the planetary gear ratio from carrier to ring gear.

The planetary gear is known for having two mechanical degrees of freedom. Therefore, different ICE speeds can be realized for a given vehicle speed. This is possible by controlling the MG1 speed on the cost of electrical energy expenditure.

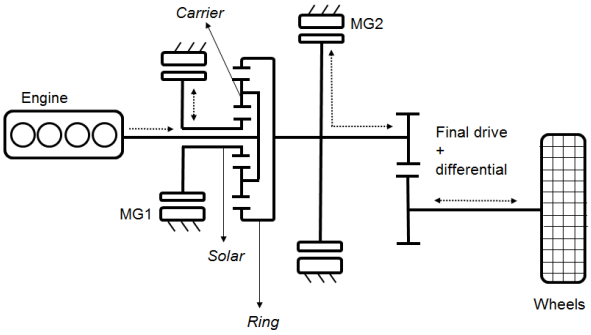

Figure 1: Diagram Of The Power-Split Hybrid Topology With Energy Flow Defined By Arrows.

The 2nd generation of Toyota Prius is the basis from where the main parameters were taken for this study. Data available for this powertrain is available in the literature (Sekimori, 1998; Kamiya, 2006; Abe, 2000). The parameters of the vehicle used in the simulation are shown in Table 1.

Table 1: Characteristics of the vehicle model.

Engine	
Displacement	1.5 dm³
Torque	115 Nm @ 4200 rpm
Power	57 kW @ 5000 rpm
Traction motor (MG2)	
Type	AC Permanent Magnet Motor
Torque	400 Nm
Power	50 kW
Maximum speed	6500 rpm
Generator (MG1)	
Type	AC Permanent Magnet Motor
Power	30 kW
Maximum speed	10000 rpm
Battery	
Type	Ni-MH
Nominal voltage	201.6 V
Rated capacity	6.5 Ah

3. SYSTEM MODELLING

The Series-Parallel configuration shown in Figure 1 allows the system to operate as an electric continuous variable transmission (CVT) since the generator is used to control the ICE speed. The torque relationship in the planetary carrier is fixed by the ratio between the diameters of each gear and a general transmission ratio of the planetary gear set, i_{PGS}, is defined as the ratio between the number of teeth of ring and sun gears. The dynamic equations for the system are shown in Eq.(1) and Eq.(2), where subscripts C, S, R, represent carrier, sun and ring gear parameters. Inertia terms from the planetary are represented by I_S, I_R and I_C, while I_{ICE}/α_{ICE}, I_{MG1}/α_{MG1} and I_{MG2}/α_{MG2} represent inertia and angular acceleration of ICE, MG1 and MG2, respectively. The equivalent rotational inertia of the vehicle mass on the shaft of the ring gear is represented by I_{R-EQ}.

$$T_{MG1} - I_S\alpha_{MG1} = -\left(\frac{1}{i_{PGS}+1}\right)\cdot\left(T_{ICE} - I_C\alpha_{ICE}\right) \quad (1)$$

$$\left(\frac{i}{i_{PGS}+1}\right)\cdot\left(T_e - I_{ICE}\alpha_{ICE}\right) + T_{MG2} - I_R\alpha_{MG2} =$$

$$= \frac{T_{W-R}}{i_{MG2-wheel}} - I_{R-EQ}\alpha_{MG2} \quad (2)$$

The ratio of angular speed between the sun, carrier and ring gear is derived by the equation below, showing the 2 degrees of freedom in the system.

$$(i_{PGS}+1)\cdot\omega_{ICE} = \omega_{MG1} + i_{PGS}\cdot\omega_{MG2} \quad (3)$$

For a given wheel speed, there will be a number of possibilities for engine and generator speeds due to the 2 degrees of freedom. In this way, MG1 will be responsible for controlling the engine speed by the cost of electrical energy.

4. POWERTRAIN PLANT MODEL

This section describes the computational implementation of the different sub-systems of the powertrain plant model.

The software MATLAB/SIMULINK™ was used for the development of the highly detailed powertrain

model. This computational model contains the following components:

- Driver model
- Engine
- Battery
- MG1
- MG2
- Transmission

The ICE model does not incorporate thermo-mechanical or combustion phenomena, and therefore, behaviors derived from catalyst and coolant warm-up are neglected. The engine subsystem incorporates a friction model and idle controller and receives an external torque request from the ICE control system. Engine friction is based on the model proposed by Chen and Flynn (1965) where the resistance load is subject to a constant term, and two terms dependent on the rotational speed and its square.

Regarding ICE fuel consumption data, in Duoba, Ng, and Larsen (2000), a torque sensor was added to the engine output shaft and torque measurements were executed in the vehicle at steady state speeds. The results, however, do not cover the whole operation range of the engine, but, instead, only the resulting operating points from the control strategy.

In order to reproduce the efficiency map of the engine, a thermodynamic engine model was created in the GT-Power software and combustion characteristics where calibrated throughout the engine speed and torque in order to result in the Brake Specific Fuel Consumption (BSFC) map shown in Figure 2. The optimum operation line (OOL) for this efficiency map is also shown in the graph.

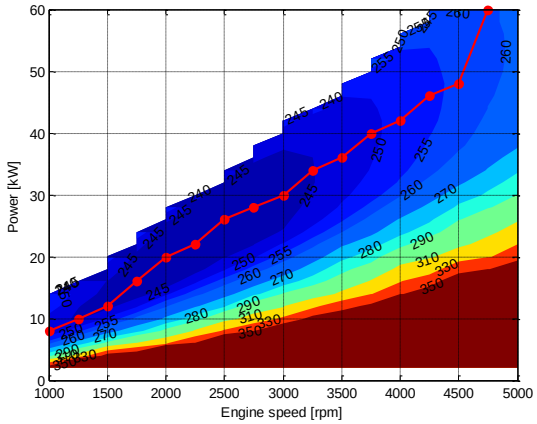

Figure 2: Engine BSFC Map And Optimum Operation Line.

The OOL in Figure 2 produces a fixed correspondence between engine speed and torque and, therefore, it reduces the system from Eq. (3) to only one degree of freedom.

An investigation conducted by Hsu et al. (2005) in order to determine the continuous torque values of the traction motor that produces a limited winding and oil temperature for a certain inlet coolant temperature shows a continuous torque of 167Nm for an inlet coolant temperature of 34.6˚C. Moreover, the peak rated capacity generates a rise in winding temperature of 2.1 °C/s.

The battery model is created using a capacitor as voltage source with internal and parasitic losses. As shown in Ehsani and Emadi (2005), the terminal voltage of such a battery is defined as:

$$V_T = V_{OC} - R_i \cdot I \tag{4}$$

where V_{OC}, R_i and I are the open circuit voltage, internal resistance and terminal current, respectively. The sum of terminal current and leakage current of the battery can be expressed as:

$$I + I_L = -C\frac{dV_{OC}}{dt} \tag{5}$$

where C is the capacitance of the battery. The leakage current is defined by V_{OC} / R_L and, when substituted in Eq. (4) and Eq. (5), it leads to:

$$\frac{dV_{OC}}{dt} = -\left(\frac{V_{OC}}{CR_L} + \frac{I}{C}\right) \tag{6}$$

The resultant battery model in Simulink from this system of equations is shown in Figure 3.

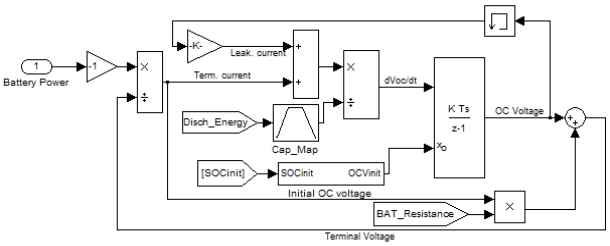

Figure 3: Battery Model In Simulink.

5. DETAILED CONTROL MODEL

This section describes the control system of the detailed powertrain model, which is composed by the following sub-systems:

- State selection
- Torque Demand calculation
- MG1 speed control
- MG2 torque control
- MCI torque control

The model developed in MATLAB™ for the control system contains a high number of sub-systems and block diagrams. It is not possible to provide all the block diagrams in the paper due to lack of available space and, therefore, only some sub-systems were made available in the APPENDIX. For complete details on

the full model, please access Trindade (2016) and Trindade, Fleury and Vogelaar (2014).

Since the simulation of the detailed model is explicit, a driver model was developed so that the speed profile of the target driving cycle could be met. A proportional-integral (PI) controller calculates the driver torque demand based on the desired and actual vehicle speeds as shown by the equation below.

$$T_{c,p}(k) = \left(V_{ref}(k) - V(k)\right) \cdot K_{p,c} + K_{i,c} \cdot t_s \sum_{k=0}^{k} \left(V_{ref}(k) - V(k)\right) + T_{ant,p}(k) \quad (7)$$

Where $T_{c,p}$ is the driver demand torque, V_{ref} is the desired speed, K_p e K_i are the controller gains, t_s is the simulation time step size, k is the instantaneous discrete time and N is the total number of discrete steps. The feed-forward term, T_{ant}, is based on the road resistance forces as shown below. An anti-windup term was incorporated to the driver model in order to prevent torque outputs outside the limits of what the real powertrain can provide.

$$T_{ant,p}(k) = \left(M \cdot r_p{}^2 + I_{TR}\right) \cdot \dot{\omega}_p(k) + \left(0.5 \cdot C_d \cdot \rho_{ar} \cdot A \cdot V(k)^2 + c_R \cdot M \cdot g\right) \cdot r_p \quad (8)$$

Figure 4 shows the difference between target and simulated speed for the NEDC cycle. The absolute difference throughout the cycle is below 0.3 km/h which indicates proper modelling of the sub-system.

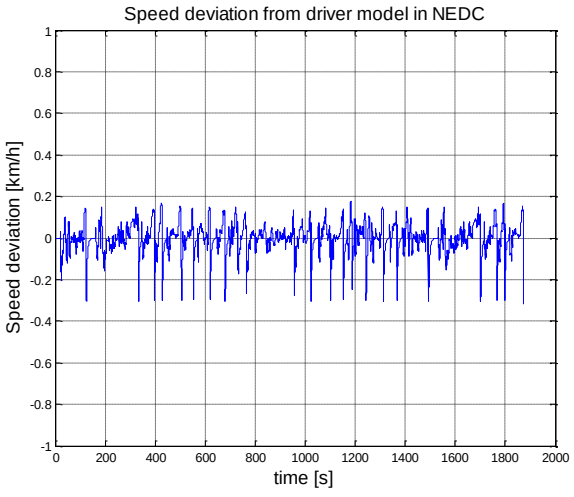

Figure 4: Absolute Speed Error From PID In Driver Model.

The state machine of the controls model defines working state of ICE and MG1. Out of electric only propulsion, the ICE has to be started and, therefore, MG1 has to operate in speed control. In order to achieve a robust control of the system, the control state of MG1 was separated into 3 sub-states: i. Sleep (no speed control); ii. ICE cranking; and iii. ICE optimum speed control. In the state machine, the ICE is activated when the driver power demand is higher than 8 kW or at vehicle speeds higher 60 km/h. This data is originated from Argonne National Laboratory (2013) and is shown in the APPENDIX.

For the speed control of MG1, a certain ICE desired speed, $\omega_{MCI,ref}(k)$ generates a desired MG1 speed, $\omega_{MG1,ref}(k)$, and the controller output will be the desired torque for MG1, $T_{MG1}(k+1)$. A PI controller as shown below was used for the speed control of MG1.

$$T_{MG1}(k+1) = \frac{T_{MCI}(k)}{i_p + 1} + \frac{\left(\omega_{MG1,ref}(k) - \omega_{MG1}(k)\right)}{\tau_{MG1}} \cdot \left(I_{BP} + I_S + I_{MG1}\right) + \left(\omega_{MG1,ref}(k) - \omega_{MG1}(k)\right) \cdot K_{p,MG1} + K_{i,MG1} \cdot \sum_{k=0}^{k} \left(\omega_{MG1,ref}(k) - \omega_{MG1}(k)\right) \quad (9)$$

Where I_{BP}, I_S e I_{MG1} represent the moment of inertia of carrier gear, sun gear and MG1, respectively, $K_{p,MG1}$ and $K_{i,MG1}$ are the controller gains and τ_{MG1} is a time constant equal to 0.1 s. The first 2 terms on the right of the equation are a feed forward part corresponding to the engine torque being transferred from the carrier to the sun gear and the resistance created by the rotational inertias in the system. The control model also restricts the maximum torque and the maximum desired acceleration of MG1 as shown in the equations below. The model of MG1 control is shown in Figure 13.

$$\frac{\omega_{MG1,ref} - \omega_{MG1}}{\tau_{MG1}} \in [-1000, 1000]\ \text{rad/s}^2 \quad (10)$$

$$T_{MG1} \in [-45, 45]\ \text{Nm} \quad (11)$$

In the ICE control system, there is a sub-module for calculation of the desired optimum engine speed generated by the desired engine torque. The final torque request to the engine is generated by the actual engine speed correlated to the OOL in a sub-module of the control system. The control system of the ICE is shown in Figure 14 of the APPENDIX.

Figure 15 of the APPENDIX shows the control system for MG2. The desired torque for MG2 has to fulfill the difference between driver torque demand and ICE delivered torque. Therefore, during electric only propulsion, when the ICE torque demand is zero, MG2 corresponds to the driver torque demand, while in

hybrid mode, the torque request for MG2 corresponds to the extra power necessary for propulsion

6. DETAILED MODEL VS MEASUREMENTS

Data from tests performed with Toyota Prius Gen 3 are available from Argonne National Laboratory (2013). This powertrain configuration has small differences in comparison with the one presented here – it includes a reduction gear between e-motor and differential - the data provides a good base for analyzing the system behavior. These data correspond to chassis dynamometer testing of the vehicle operating under the urban cycle FTP75.

As mentioned before, the simulation runs in explicit mode with the traction torque demand originated set by the driver model. Figure 5 shows vehicle and ICE speed for the simulation and test data results under the FTP75 cycle. No emission strategy is considered in this simulation, which makes the ICE operates in a start stop profile at the beginning of the cycle. Besides this difference against the test data, it is noted a high correlation of the measured and simulated engine speed. The same can be said when one analyzes the battery current signal. Battery current is analyzed in this section as it is directly related to the power-split ration between engine and e-motor.

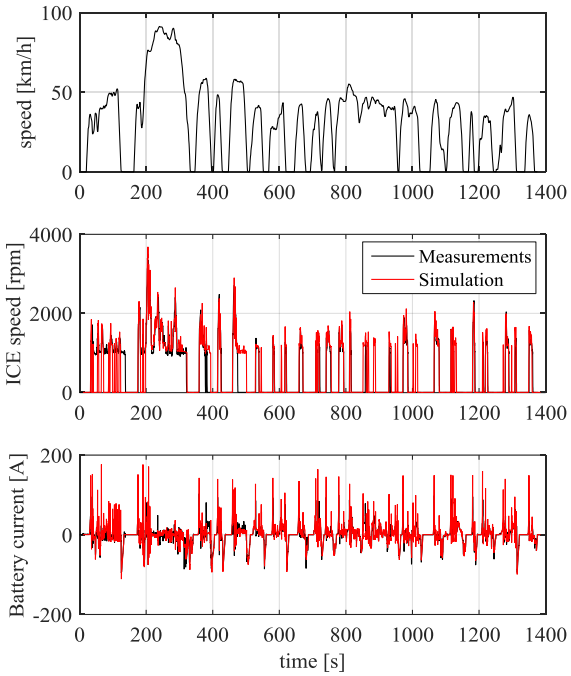

Figure 5: Comparison between detailed model and measurements: vehicle speed, ICE speed and battery current.

7. GLOBAL OPTIMAL CONTROL

Dynamic programming is an optimization algorithm which aims to finding the solution that generates the global minimum result for a given cost function. This means that for a certain driving cycle, the optimized solution will be a vector of control values against time. A time continuous function represents the current system which can be synthetized by:

$$\dot{x}(t) = f(x(t), u(t), t) \tag{12}$$

where u(t) is the control variable, in this case the power-split (PS), and x(t) is the vector of state variables of the system, in this case the battery SOC. The cost function for this system is:

$$J(u(t)) = G(x(t_f)) + \int H(x(t), u(t), t)dt \tag{13}$$

where $G(x(t_f))$ is the final cost and the second term represents a penalty to ensure that a dynamic constraint should be satisfied, in this case that the SOC at the beginning and at the end are the same. The following cost function represents the fuel consumption in the vehicle over the driving cycle:

$$J(u(t)) = \int \dot{m}_{fuel}(u(t), t)dt + (SOC_{end} - SOC_{ini})p \tag{14}$$

The constraints for the optimization have to be set in order to prevent that the system drift out of its boundaries:

$$T_{\min} < T_{req} < T_{\max} \tag{15}$$

$$SOC_{\min} < SOC < SOC_{\max} \tag{16}$$

$$SOC_{end,\min} < SOC_{end} < SOC_{end,\max} \tag{17}$$

$$u_{\min}(SOC, t) < u(SOC, t) < u(SOC, t)_{\max} \tag{18}$$

where T_{req} are the torque requests in the system for ICE, MG1 and MG2 and SOC_{end} is the SOC value at the end of the cycle.

The DP routine developed by Sundström and Guzzella (2009) was used in this analysis. The range of the PS control variable was divided in 0.1 intervals from [-1, 1], where 1 means pure electric driving, values between 0 and 1 mean electric assist drive and negative values mean hybrid generation.

Two simulation cases were generated using the dynamic programming routine. In the first case (DP 1), the only control variable to be optimized was the power-split. The engine start behavior was set according to Figure 16 and the engine follows the Optimum Operation Line (OOL) as in Figure 2. In the second case (DP 2), the engine start behavior and the engine operating points were also subject of optimization together with the power-split ratio. The intention with DP 2 was to evaluate the interconnection between the different variables and to evaluate if the best results in terms of overall powertrain efficiency are really achieved by having the engine following the OOL.

The SOC possibilities were divided in 61 steps between the 50% and 70%, which represents the usable SOC of the battery. The SOC was allowed to have a variation of -1.6%, which corresponds to the net variation in the test results. This was done in order to

have a comparable behavior with the measurements which also improves the comparison of fuel consumption results.

7. RESULTS

The different simulations and the test measurement have different values for the SOC at the end of the cycle and, therefore, it is necessary to correct the final fuel consumption value in order to account for the cost of battery energy. The factor used for the corrections was 340 g of fuel per kWh of battery energy. This value was obtained by observing the average values of engine, transmission, electric motors and battery efficiency during the cycle.

Figure 6 shows the results for the fuel consumption and state variable trajectories during the cycle. The resultant SOC trajectory for the detailed model does not present a high correlation with the measurement data, which shows the limitation of a rule based control strategy in order to replicate a real and complex system. On the other hand, the SOC trajectory of the DP 1 is curiously similar to the test measurements, except for a deviation in the first 350 s of the cycle, which is most probably due to warm-up strategies that have the engine running continuously rather than following the control strategy in the tests.

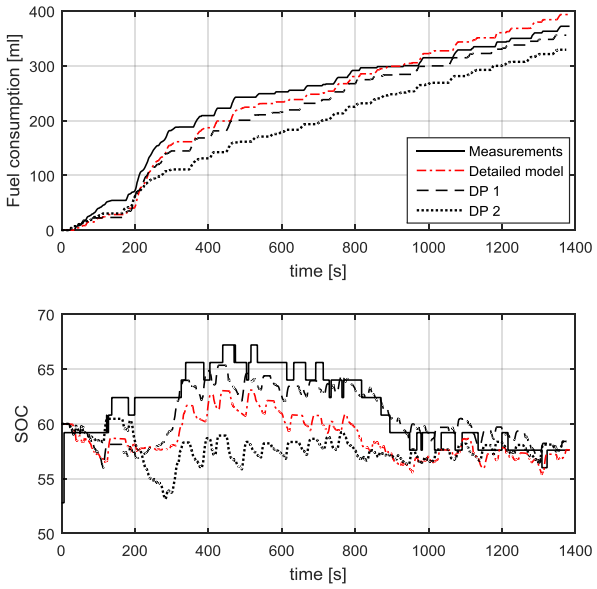

Figure 6 – Fuel consumption (top) and SOC (bottom) trajectories for measurements, detailed model, DP 1 and DP 2.

Figure 7 shows the final fuel consumption for all the simulations and for the test measurement. The detailed model had a final fuel consumption 6.75% above the measurements. This is an expected result as a heuristic control strategy is known for not providing results close to the system minimum. Additionally, from the SOC trajectory in Figure 6, it is strongly believed that the real vehicle has an optimized control strategy since the measurement result was very close to DP 1.

The result for DP 1 was 4.5% below the measured data, which is an acceptable difference since most of the simulation parameters were taken from the literature and the model results could only be compared to measurements on the system level rather than on the component level. The fuel consumption result for DP 2 was 7.5% lower than DP 1, indicating a high efficiency gain due to the extra optimized variables. The reason for the differences will be discussed further in this document.

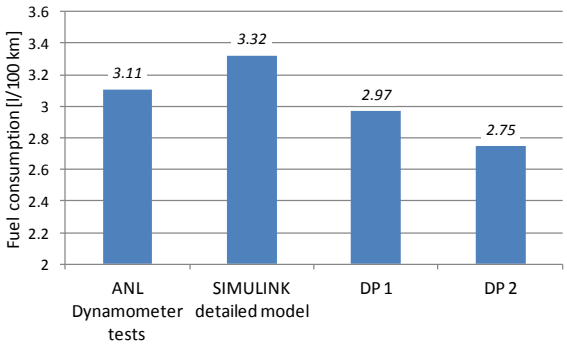

Figure 7 – Fuel consumption results for measurements, detailed model, DP 1 and DP 2.

Figure 8 shows the energy on the different hybrid modes for the different simulations. The "Engine" energy corresponds to the mechanical energy of the ICE, while the energy in EV (pure electric propulsion), Regeneration, Hybrid Boost (or assist) and Hybrid Generation corresponds to the electrical energy at the battery terminal.

From Figure 8, it is noticed that DP 1 prioritises EV driving in comparison with the Detailed model and uses less engine energy. Moreover, DP 1 provides more energy to the battery via Hybrid Generation in order to extend EV driving. Regarding DP 2, there is a trend to use even less "Engine" energy by operating more in "Hybrid Boost" and less in "EV" mode.

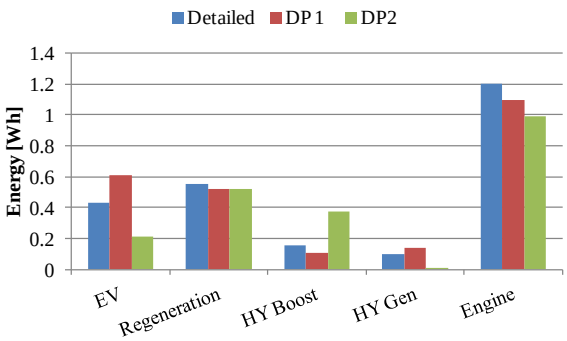

Figure 8 – Result of energy consumption (absolute values) from simulations for the different hybrid modes.

Figure 9 shows the engine start behavior for DP 2. The power demand at which the engine starts is now around 4 kW, instead of 8 kW as seen from the test results and implemented in the detailed mode and in DP 1. By doing this, there are less EV driving events, which explain the low EV energy.

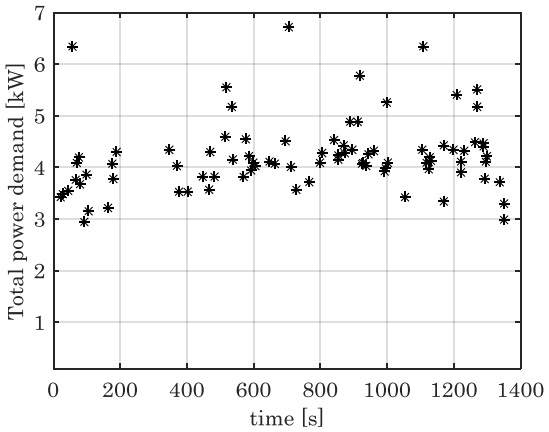

Figure 9 – Engine start behavior from DP 2.

The early engine start from DP 2 was not expected at first since low engine power demands would not directly provide high engine efficiency. The same is valid for the increased energy spent in hybrid boost mode as the hybrid controls would give priority to increase the load on the engine rather than to decrease it. However, this behavior is understood first by looking at Figure 10, which shows the BSFC for the operating points on the OOL. The minimum BSFC (242.5 g/kWh) in the graph is only around 1% better than the BSFC at low 10 kW. This indicates that increasing the load on the engine (hybrid generation) only provides a small increase in engine efficiency and that the increase in overall powertrain efficiency should be lower than zero due to the losses on the electrical path.

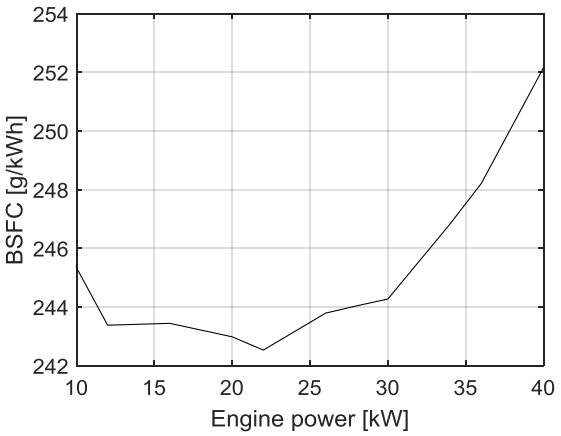

Figure 10 – BSFC of the engine at the Optimum Operation Line (OOL).

Nonetheless, perhaps the greatest advantage from DP 2 is from decreasing the "energy recirculation" in the powertrain, which occurs when electric power is generated at the MG1 to be directly consumed by MG2, or vice-versa. This is a known drawback of series-parallel hybrid with such arrangement of planetary gear. The sum of "EV", "Hybrid boost" and "Hybrid generation" energy in DP2 is lower than in DP 1, which in turn produces less electric losses. These losses do not have to be overcome by the higher "Engine" energy, increasing the overall powertrain efficiency.

Figure 11 and Figure 12 show the traction torque at the differential input for each hybrid mode. In Figure 11, the hybrid strategy results in many operating points in hybrid generation mode, which seems to be located in on the transition between EV and hybrid boost mode. This is partly due to the fact that the ICE has to follow the OOL and partly due to the high ICE start threshold, which creates the need for hybrid generation as the recuperation energy is not enough to assure charge sustaining mode. Hybrid boost mode around 50 km/h and 50 Nm were identified where the battery SOC was 3% above the target, which explains the choice of spending electrical energy even at low power demands.

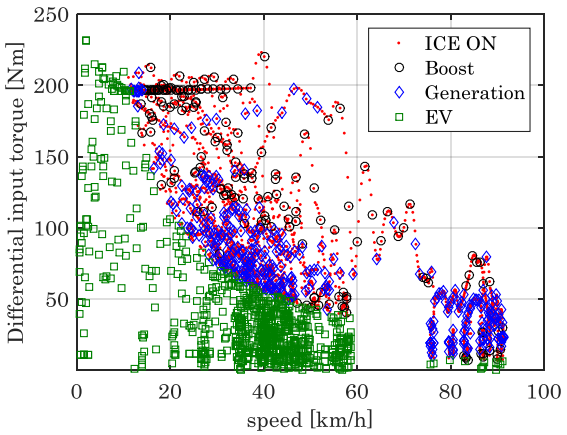

Figure 11 - Torque at the differential input shaft during traction events for different hybrid modes in DP 2.

The lower ICE ON power threshold (transition from EV to ICE ON) from DP 2 is seen in Figure 12, which also shows a much lower amount of hybrid generation points than DP 1 as indicated in Figure 8. The control strategy in this case prioritizes starting the engine earlier and use more electrical energy for propulsion in "Hybrid boost" rather than in "EV" mode. The reason for this may be to use fuel energy, since the engine efficiency would already be high enough, and also use electrical energy, since it is widely available from recuperation events.

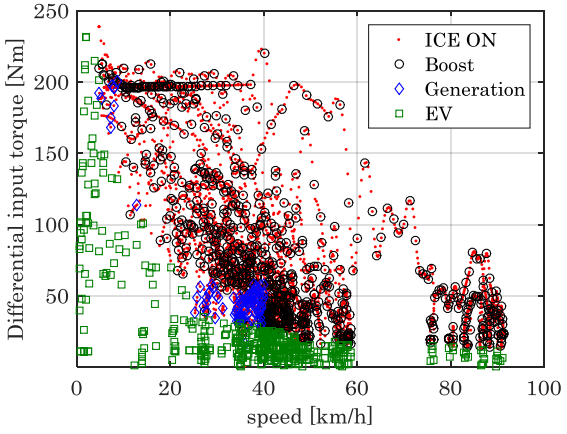

Figure 12 – Torque at the differential input shaft during traction events for different hybrid modes in DP 1.

CONCLUSION

This paper showed the development of two different powertrain models for a Series-Parallel hybrid electric vehicle: 1. A detailed powertrain model using heuristic control laws and 2. A model using global optimum control implemented via a dynamic programming (DP) routine. The DP model simulation comprised two different cases aiming to further explore the total fuel economy potential of the system by finding optimal values for additional control variables. Chassis dynamometer data from the baseline vehicle was also used to assist the development of the models.

From the results of the first simulation case of the DP routine (DP 1), it was identified in Figure 6 that the real vehicle has a very similar response to a globally optimized system. This points out that the fuel consumption deviation of 6.75% between the detailed model against the real vehicle is acceptable, since the control in the simulation uses a rule based approach.

From the measurement data, it was identified that the real vehicle controls the engine by having it operating on its optimum operating line (OOL) in order to maximize engine efficiency. This strategy was implemented in the detailed model and in DP 1, however, differently from DP 1, in the second case of the DP routine (DP 2), the engine operation was set not to follow the optimum operating line but was free to be optimized. Besides that, the engine start threshold was also subject of optimization. At the end, the fuel consumption result from DP 2 was 7.5% lower than DP 1, showing that optimizing the system for overall powertrain efficiency provides an extra fuel consumption benefit against an optimized system focusing on engine efficiency. This improved result was achieved by actively reducing the losses on the electrical path, consequently having less load cycles in the battery.

APPENDIX

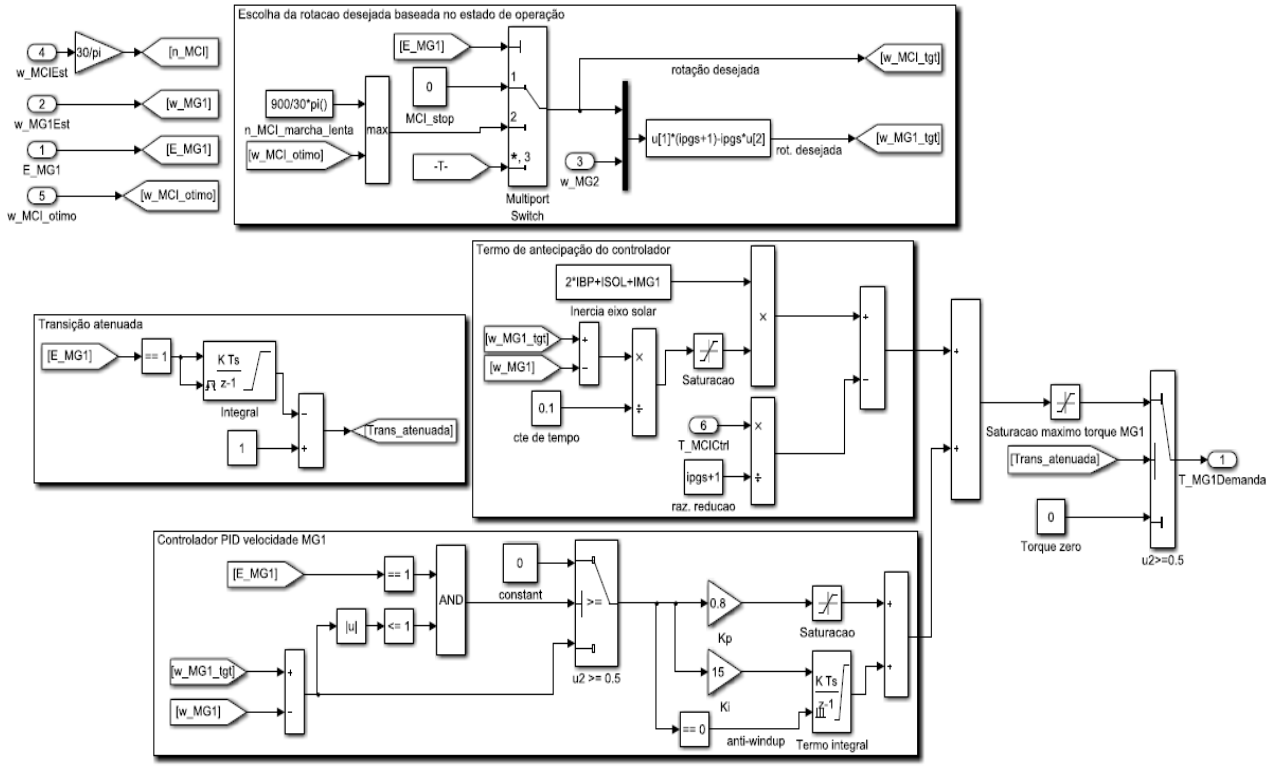

Figure 13 – MG1 control system.

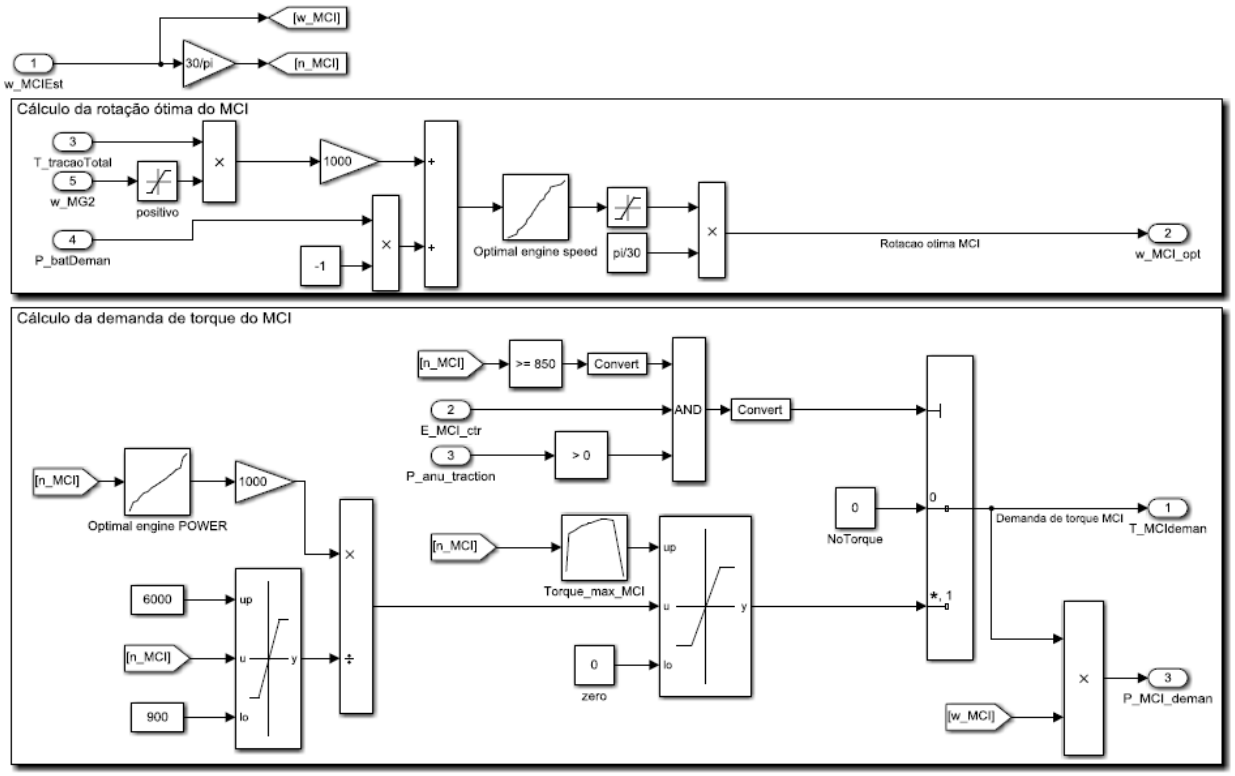

Figure 14 – Control system of the ICE.

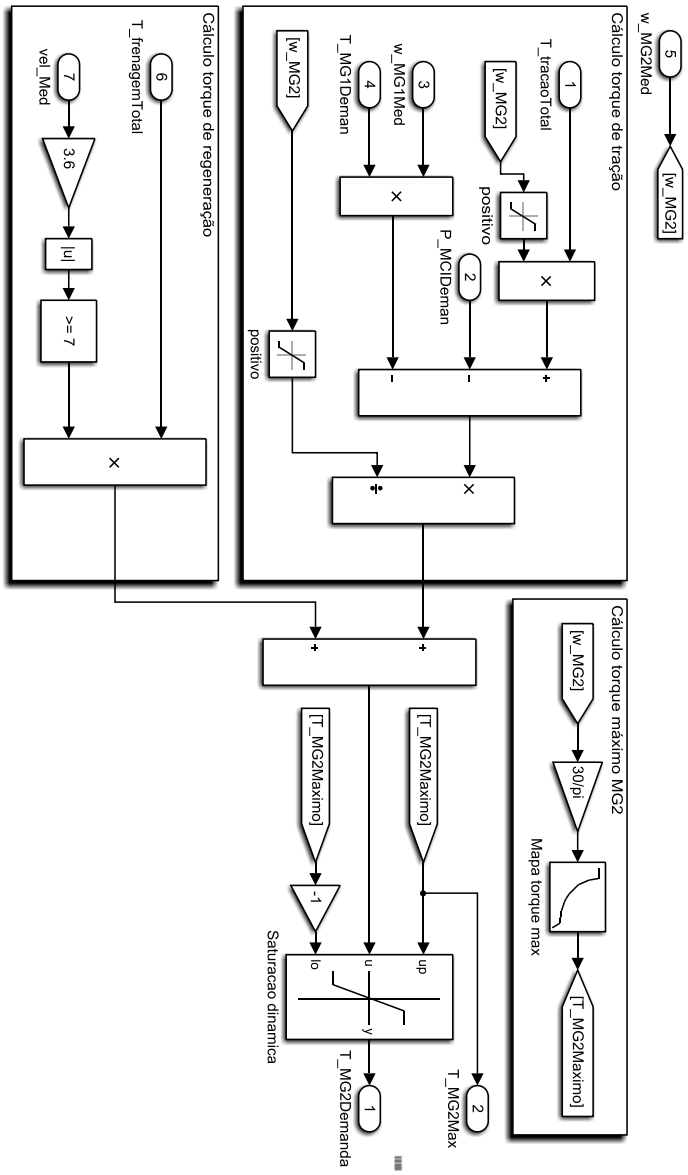

Figure 15 – MG2 control system.

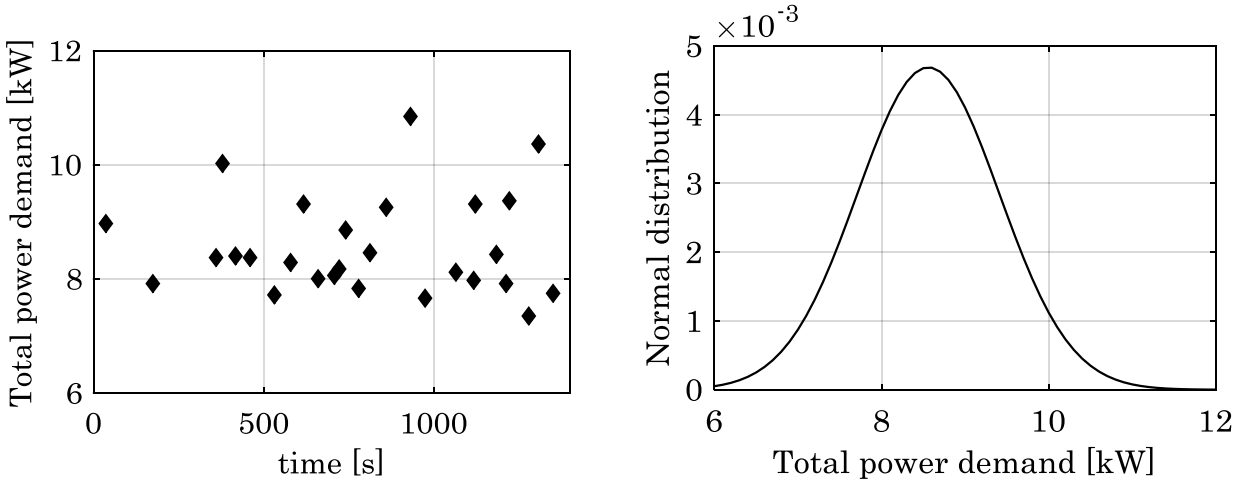

Figure 16 - Test results for engine start behavior (Argonne National Laboratory, 2015).

REFERENCES

Abe S., 2000. Development of the Hybrid Vehicle and its Future Expectation. SAE Technical Paper 2000-01-C042.

Argonne National Laboratory, 2013. All Data- 2010 Toyota Prius, Available from: http://www.anl.gov/energy-systems/group/downloadable-dynamometer-database/hybrid-electric-vehicles/2010-toyota-prius, [Accessed 17 February 2015].

Ayers C., Hsu J., Marlino L., Miller C., Ott Jr.G., Oland C., 2004. Evaluation of 2004 Toyota Prius Hybrid Electric Drive System Interim Report. ORNL/TM-2004/247.

CarignanoI. M. G., Nigro, N. M., Junco, S., 2015. Hybridization Effect On Fuel Consumption and Optimal Sizing of Components For HEV. In The 8th. International Conference on Integrated Modeling and Analysis in Applied Control and Automation (IMAACA 2015). Begerggi, Italy, pp. 48–54.

Chen S. and Flynn P., 1965. Development of a Single Cylinder Compression Ignition Research Engine. SAE Technical Paper 650733.

Delprat S., Lauber J., Guerra T., Rimaux J., 2004. Control of a parallel hybrid powertrain: Optimal control. IEEE Transactions on Vehicular Technology, 53(3), 872–881.

Duoba M., Ng H., Larsen R., 2000. In-Situ Mapping and Analysis of the Toyota Prius HEV Engine. SAE Technical Paper 2000-01-3096.

Duoba M., Ng, Henry, Larse R., 2001. Characterization and Comparison of Two Hybrid Electric Vehicles (HEVs) – Honda Insight and Toyota Prius. SAE Techinical Paper 2001-01-1335.

Ehsani M., Gao Y., Emadi A., 2005. Modern Electric, Hybrid Electric, and Fuel Cell Vehicles, Fundamentals, Theory, and Design. 2nd ed. Florida: CRC Press.

Gray T., Shirk M., 2013. Toyota Prius VIN 0462 Hybrid Electric Vehicle Battery Test Results. Idaho National Laboratory INL/EXT-13-28025.

Hsu J.; Nelson S., Jallouk P., Ayers C., Campbell S., Coomer C., Lowe K., Burress T., 2005. Report on Toyota Prius motor thermal management. Oak Ridge National Laboratory, ORNL/TM-2005/33.

Kim N., Rousseau A., Rask, E., 2012. Autonomie Model Validation with Test Data for 2010 Toyota Prius. SAE Technical Paper 2012-01-1040.

Lin C., Peng H., Grizzle J., Kang J., 2003. Power management strategy for a parallel hybrid electric truck. IEEE Trans. Control Systems Technol., 11(6), 839–849.

M. Kamiya, 2006. Development of traction drive motors for the toyota hybrid system. IEEE Transactions on Industry Applications, 126(4), 473-479.

Muta K., Yamazaki M., Tokieda J., 2004. Development of New-Generation Hybrid System THS II - Drastic Improvement of Power Performance and Fuel Economy. SAE Technical Paper 2004-01-0064.

Rask E., Duoba M., Busch H., Bocci D., 2010. Model Year 2010 (Gen 3) Toyota Prius Level-1 Testing Report. Argonne National Laboratory. Report ANL/ES/RP-67317.

Sekimori T., 1998. Development of Toyota's Electric and Hybrid Vehicle. SAE Technical Paper 98C053, 355-361.

Sundström O., Guzzella L., 2009. A Generic Dynamic Programming Matlab Function. Proceedings of the 18th IEEE International Conference on Control Applications, 1625–1630, Saint Petersburg, Russia.

Trindade I, 2016. Modelagem, Controle e Otimização do Consumo de Combustível Para Um Veículo Híbrido Elétrico do Tipo Serie-Paralelo. Master's Thesis. Polytechnic School, University of Sao Paulo. Available from: www.teses.usp.br.

Trindade I., Fleury, A., 2015. Modeling, control and application of dynamic programming to a series-parallel hybrid electric vehicle. In The 8th. International Conference on Integrated Modeling and Analysis in Applied Control and Automation (IMAACA 2015). Begerggi, Italy, pp. 71–78.

Trindade I., Fleury, A., Vogelaar, G.-J., 2014. Modeling, Simulation and Analysis of Operation Modes in a Series-Parallel Hybrid Electric Powertrain With Torque-Split Device. SAE Technical Paper 2014-36-0351, Sao Paulo.

AUTHORS BIOGRAPHY

Ivan Miguel Trindade has a Master's degree from Polytechnic School of University of São Paulo and a degree in mechanical engineering (2008) from the same university. He has worked on various projects related to internal combustion engines and hybrid powertrain development. He currently works for AVL Schrick GmbH covering a variety of tasks involving hybridization and electrification of automotive powertrain.

Agenor de Toledo Fleury has a degree in mechanical engineering from ITA - Technological Institute of Aeronautics (1973), a MSc (1978) and a PhD degree (1985) in Mechanical Engineering from the University of São Paulo. He is currently an assistant professor at Polytechnic School, University of Sao Paulo. He has previously served the Brazilian Institute for Space Research (INPE), the Brazilian Aeronautic Enterprise (EMBRAER), the Sao Paulo State Institute for Technological Research (IPT) and FEI University, leading various projects with emphasis on Dynamics and Control Systems. His most recent projects address modeling and control of nonlinear systems, optimal control and estimation, in applications of Biomechanics, Robotics and Automotive Engineering.